RSC Advances

ROYAL SOCIETY OF CHEMISTRY

www.rsc.org/advances

RSC Advances

PAPER

Fabrication and biocompatibility of reduced graphene oxide/poly(vinylidene fluoride) composite membranes

Received 00th January 20xx,
Accepted 00th January 20xx

DOI: 10.1039/x0xx00000x

www.rsc.org/

Supeng Pei[a]*, Fei Ai[b] and Song Qu[c]

The graphene/polymer composite membranes were prepared by an in-situ thermal reduction method and their biocompatibility was evaluated. Brown graphite oxide (GO)/poly(vinylidene fluoride) (PVDF) composites were initially prepared by solution processing, then converted to black membranes through compression molding at 200 °C. Structural analyses indicated that GO was reduced and well dispersed in PVDF matrix during the processing course, and revealed a wrinkled topography of the reduced graphene oxide (RGO). Incorporation of RGO facilitated the formation of *β* phase PVDF and increased its wettability. Cell culture results showed that human umbilical vein endothelial cells (HUVECs) spread and proliferated much better on the composite membranes, indicative of promoted cell adhesion and proliferation and enhanced biocompatibility of the membranes. Such excellent performance of the RGO/PVDF composite membranes makes them promising candidates as biomaterials.

1 Introduction

Graphene, the basal plane of graphite, is composed of hexagonally arrayed sp^2-bonded carbon atoms. Due to its exceptional optoelectronic and mechanical properties, outstanding thermal stability, biocompatibility and diverse applications in field-effect transistors, solar cells, sensors, supercapacitors, biocomposites, and so on, it is attracting increasing research attentions.[1-15] Specifically, graphene sheets (GSs) can be used as fillers to dramatically improve mechanical, electrical, thermal, gas permeation, and other properties of the polymer matrix.[16,17]

Poly(vinylidene fluoride) (PVDF) is a well known and extensively studied polymer because of its outstanding dielectric, piezoelectric, pyroelectric and ferroelectric properties. With exceptional chemical resistance, wonderful thermal stability and biostability, PVDF has been employed as biomaterials, such as soft tissue repair and structure materials with excellent biocompatibility.[18,19] The inherent hydrophobicity, however, makes it difficult to interact with cells and tissues, and thus dramatically limited its biomedical applications. Many methods were developed to improve its surface hydrophilicity, including blending with suitable acrylic resins and surface grafting.[20-25] Moreover, as a semi-crystalline polymer, PVDF exhibits at least five crystalline phases, namely *α, β, γ, δ* and *ε* phases,[26] which may evoke different cellular behaviors.[27] Recently, it is found that addition of GSs to the PVDF matrix can improve its wettability, and promote the formation of *β* phase crystals.[28,29] Additionally, carbon-based materials, including carbon fibers, carbon nanotubes, and graphene, are well accepted by the biological environment, and may stimulate cell growth.[30,31] It is thus expected that GS/PVDF systems can be used for biological applications. However, GSs tend to adhere to each other because of the high cohesive strength caused by van der Waals energy, and are thus difficult to be dispersed into the polymer matrix without agglomeration. Subsequently, graphene based composite materials are almost prepared in dilute solutions, which dramatically restricts their applications. In this study, we endeavoured to develop an easy approach to fabricate graphene-based composites for biomedical applications.

Initially, graphene was prepared by mechanical exfoliation. Though many other methods, such as chemical vapor deposition, arc discharge, epitaxial growth, micromechanical exfoliation and reduction of graphite oxide (GO) have been developed to obtain graphene, exfoliation and reduction of GO is considered as the most promising one for large scale production. GO is normally synthesized by chemical oxidation of graphite, which introduces oxygen-containing functional groups to exfoliate pristine graphite sheet.[32] The single-layered GO exfoliated by ultrasonication is so called graphene oxide. Reduction of GO can be realized by chemical methods, using such reductants as hydrazine,[33] dimethylhydrazine,[34] ascorbic acid,[35] pyrrole,[36] aluminum powder[33] and gaseous H_2[38]. Thermal reduction is another mean, which is believed to be green because no hazardous reductants are used.[27] Exfoliation is caused by the expansion of CO_2 evolved in the interstices between graphene sheets during rapid heating.[28] Exfoliation takes place when the decomposition rate of epoxy and hydroxyl sites of GO exceeds the diffusion rate of the evolved gases, thus yielding pressures over the van der Waals forces between GSs.[39] The heating temperature significantly affects the reduction degree of GO.[40,41] Normally, high reduction temperatures are

[a] School of Chemical and Environmental Engineering, Shanghai Institute of Technology, Shanghai 201418, China.
[b] School of Chemistry and Chemical Engineering, Shanghai Jiao Tong University, Shanghai 200240, China.
[c] College of Science, University of Shanghai for Science and Technology, Shanghai 200093, China.
†*Corresponding author E-mail: peisupeng@126.com, Tel: +86-21-60877214 Fax: +86-21-60877231

needed to achieve excellent reduction degrees. However, even when the temperature is as high as 1 100 °C, the oxygen-containing functional groups still cannot be completely eliminated. Fortunately, it is great that there is remarkable reduction of GO even at a relatively low temperature of 200 °C.[39,42] With some residual functional groups and defects, the reduced graphene oxide (RGO) sheets can be considered as one kind of chemically derived graphene.

According to the above thermal reduction and expansion mechanism, an easy in-situ thermal reduction method was utilized to prepare RGO/PVDF composites from the GO/PVDF blends, which were prepared by solution processing. Structure and surface topography of the membranes were thoroughly investigated. Human umbilical vein endothelial cells (HUVECs) were cultured on the pristine and composite membranes to evaluate the adhesion and proliferation behaviors induced by the incorporation of graphene.

2 Experimental

2.1 Materials

Natural graphite, 12 000 mesh, was kindly provided by Qingdao Ruisheng Graphite Co. Ltd (China). PVDF powder (FR902) was supplied by Shanghai 3F Ltd. (China). Other reagents were purchased from Sinopharm Chemical Reagent Co. Ltd. (China) and used as received.

2.2 Fabrication of composites

GO was prepared from natural graphite powder by a modified Hummers method,[26] and the C:O ratio is 2.6 as determined by X-ray photoelectron spectroscopy (XPS). GO slurry was dried at 50 °C in a vacuum oven, then the weighted power was dispersed in *N,N*-dimethylformamide (DMF) by ultrasonication for 30 min. DMF solution of PVDF (15%) was then mixed with GO dispersions, and the final concentration was adjusted to 10%. After being stirred for 30 min, the mixture was ultrasonicated for another 30 min. Then the GO/PVDF hybrid solution was dried in vacuum at 60 °C. RGO/PVDF membranes were prepared by compression molding (200 °C, 10 MPa, 10 min). Some holes emerged on the membrane surface after the first compression, indicating GO thermal reduction induced masses of gases emission during the first circle. Such holes were increased with increasing GO amount, and almost disappeared after the second circle. To get a smooth membrane, each sample was compressed twice. Six sets of GO/PVDF samples with GO loadings of 0.5, 1, 2, 4, 8 and 10% were prepared and the resulting hot-compressed RGO/PVDF composite membranes are named as G0.5, G1, G2, G4, G8 and G10, respectively. Because of being enveloped by PVDF, GO will not be oxidized in air at high temperatures, making it an effective method to avoid the interference of oxygen. During the compression course, the evolved gases from GO rapidly diffuse and exfoliate the RGO sheets; simultaneously, melted PVDF enters into the RGO gaps and stabilizes the dispersed RGO sheets. Owing to the low reduction temperature of 200 °C, the reduction degree of GO is relatively low, making some oxygen-containing functional groups still existed in the resulting RGO sheets.

2.3 Characterization

Transmission electron microscopy (TEM) observations were taken on JEM-2100 (JEOL, Japan). Atomic force micrographs (AFM) were obtained using a Nanonavi E-Sweep (Seiko, Japan) in tapping mode. Crystalline structure of the composite membranes was monitored by X-ray diffraction (XRD) analysis (Rigaku D/max-2200/PC system). The radiation source (Cu Kα X-ray) was operated at 40 kV and 20 mA, with the scanning angle over the range of 5–45° (2θ) and a scanning velocity of 4° min^{-1} at room temperature. Differential scanning calorimetry (DSC) experiments were performed on Q2000 (TA Instruments, USA) under nitrogen.

Contact angles were measured on an OCA 20 Contact Angle System (Data Physics Instruments GmbH, Germany) with distilled water at 25 °C and 45% relative humidity (RH). Herein reported data are the average values of 6 measurements taken at different positions with 2 μL of liquid. Surface chemical composition was determined by X-ray photoelectron spectra (XPS, AXIS Ultra DLD, Shimadzu, Al source, take-off angle: 90°). The high-resolution C1s spectra were deconvoluted and fitted to analyze the chemical composition.

2.4 Cell adhesion and proliferation assay

The composite membranes were prepared in 1.6-cm circular shape for cell culture, sterilized by alcohol (70%), and then placed in a 0.1 M phosphate-buffered solution (PBS). The samples were placed in 24-well plates filled with Dulbecco's minimal essential media (DMEM) (GIBCO BRL, USA) supplemented with 10% fetal bovine serum. HUVECs were seeded on membranes at a density of 5×10^4 cells/sample. Then the culture plates were kept in a CO_2 incubator (Thermo Forma® 3111) at 37 °C. HUVEC proliferation was detected by a commercial WST-1 Kit (Beyotime Institute of Biotechnology), which is a modified MTT assay. A digital camera attached to a microscope (Nikon, Ti) was used to capture images of cells stained by acridine orange/ethidium bromide (AO/EB).

3 Results and discussion

3.1 Morphology of GO

Optical observation is a direct way to trace the changes of GO in the composites. Fig. 1 presents the photographs of the samples at each step. While initial GO/PVDF hybrid solution and membranes are brown (Fig. 1A and 1B), the color of the hot-compressed membrane becomes black (Fig. 1C), indicating the reduction of brown GO to black RGO or grapheme segments. Fig. 2A and 2B depict the GO/PVDF membrane before and after compression. Clearly, the thermal compressed GO presents a metallic luster compared to its precursor with a brown color, which also suggests the restore of graphene structure.[41] TEM image reveals the tightly stacked GO sheets in solution (Fig. 2C). However, after hot-compression, such stacked sheets are successfully exfoliated, showing a wrinkled topography of single-layered sheets (Fig. 2D), which is quite in agreement with the reported GS morphologies.[43]

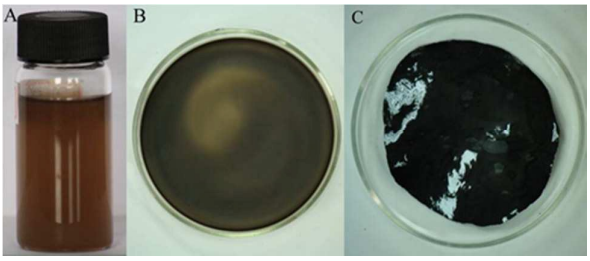

Fig.1 Photographs of (A) GO/PVDF in DMF, (B) GO/PVDF membrane and (C) hot-compressed G0.5 membrane.

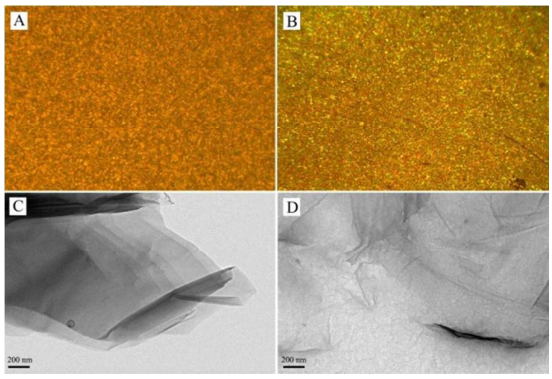

Fig. 2 Metallurgical microscope images of (A) GO/PVDF solution cast membrane and its (B) hot-compression molded membrane with 8% GO loading (×200). TEM images of the GO/PVDF solutions (8% GO) from corresponding membranes (C) before and (D) after hot-compression.

Raman spectroscopy is a powerful tool to determine the quality of GSs. Fig. 3 compares the Raman spectra of varying composite membranes with 8% GO loading. All composite membranes display two prominent peaks at ~1330 and ~1590 cm^{-1}, which are corresponded to the D and G bands, respectively. While the G band corresponds to the first-order scattering of the E_{2g} mode observed for sp^2 carbon domains, the D band is ascribed to the disordered band associated with structure defects of graphene. Therefore, the area ratio of D band to G band (I_D/I_G) is usually used to evaluate the disorder degree.[44] There is a slight decrease of I_D/I_G after hot compression (from 0.84 to 0.78), thus indicating the restore of graphene structure. Meanwhile, through further annealing, I_D/I_G is decreased to 0.64, suggestive of more ordered structure of RGO.

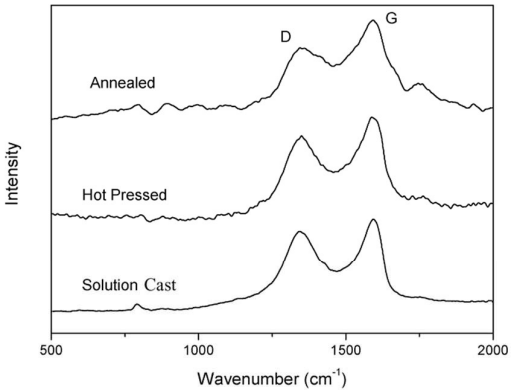

Fig. 3 Raman spectra of different composite membranes with 8% GO loading.

3.2 Crystalline structure analysis

Microstructures of the composite membranes were studied by XRD. For the hot-pressed pure PVDF membrane, three featured peaks at 2θ = 17.6, 18.4 and 19.90° are observed (Fig. 4A), corresponding to the planes (1 0 0), (0 2 0) and (1 1 0) for α phase,[28,29] respectively. When dried at 80 °C, the GO/PVDF membrane displays a GO diffraction peak at ~9.0°, from which the *d*-spacing is derived to be 0.98 nm. However, after being compressed at 200 °C, the GO diffraction peak is disappeared, indicating the reduction of GO and well dispersion of RGO in the PVDF matrix; Meanwhile, a new peak at 2θ = 20.6° corresponding to the planes (110) and (200) for β phase PVDF emerges. For graphite (1%)/PVDF membrane, a characteristic graphite peak at 2θ = 26.4° is observed (Fig. 4B). And the absence of such peak for RGO/PVDF membrane suggests no accumulation and thereby well-distribution of RGO. With increasing graphene content, the β characteristic peak intensity of PVDF at 20.6° is increased (Fig. 4C), indicating RGO can promote the formation of β phase PVDF. Furthermore, through annealing at 100 °C for 60 min, the relative peak intensity of β (110) and (200) is significantly increased (Fig. 4D), indicating the crystal transformation from α to β phase.

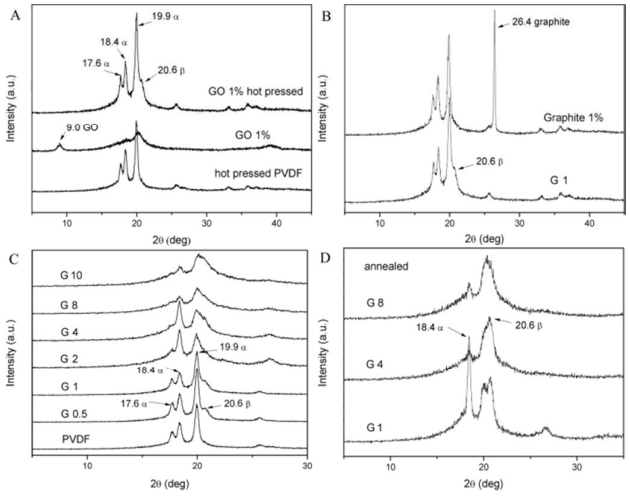

Fig. 4 XRD patterns for (A) PVDF, GO/PVDF membranes before and after compression molding, (B) G1 and graphite (1%)/PVDF membranes, (C) composite membranes with varying RGO contents and (D) annealed composite membranes.

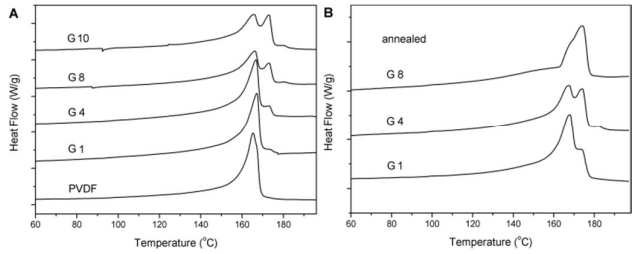

Fig. 5 DSC thermograms of (A) hot compression molded RGO/PVDF and (B) their corresponding annealed membranes.

DSC measurement was utilized to evaluate the effects of RGO and thermal annealing on the crystalline structure of PVDF. As depicted in Fig. 5, while pristine PVDF exhibits a single melting peak at 165 °C, RGO/PVDF membranes show two melting peaks at 165 and 173 °C, which are corresponded to α and β phases of PVDF, respectively.[28] The relative peak intensity at 173 °C is greatly enhanced with increasing RGO content, suggesting RGO can promote the transformation of PVDF from α to β phase (Fig. 5A), which well agrees with above XRD results. The added graphene sheets are probably acting as nucleating agent by providing large surface area for adsorption of PVDF chain and thereby causing easier nucleation and more β fraction.[28,29] Through further thermal annealing, more α-PVDF is converted to β phase (Fig. 5B), which is consistent with the XRD result.

3.3 Surface property

Surface property of biomaterials has great influence on protein adsorption and cell adhesion. To determine the hydrophilicity of

RGO/PVDF membranes, on which water contact angles were measured. Fig. 6 illustrates the typical water drop profiles on pure PVDF and RGO/PVDF composite membranes. The contact angles are 84.8, 80.7, 79.3 and 78.4° for PVDF, G1, G4 and G8 membranes, respectively. The data are the average values of 6 measurements (Table 1) taken at different positions with 2 μL of liquid. PVDF is inherently hydrophobic, whereas RGO exhibits hydrophilicity due to the presence of such hydrophilic groups as carboxyl and hydroxyl. Incorporation of RGO into PVDF increases the membrane surface hydrophilicity, thereby leading to the decrease of contact angles. For comparison, contact angles of the annealed composite membranes were also checked. It is noted that the contact angles of G4 and G8 membranes are increased from 79.3° and 78.4° to 82.1° and 81.2° through annealing. To explore the exact reasons for such variation, XPS and AFM analyses were further conducted.

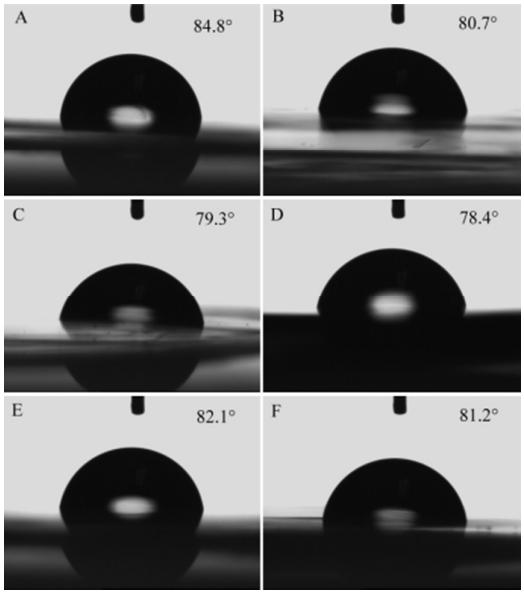

Fig. 6 Water drop profiles on (A) PVDF, (B) G1, (C) G4, (D) G8 and annealed (E) G4 and (F) G8 membranes.

Table 1 Contact angles of different samples

number	PVDF	G1	G4	G8	G4 annealed	G8 annealed
1	85.0	80.9	79.6	78.1	82.0	81.4
2	84.7	80.7	79.4	78.4	81.9	81.1
3	84.8	80.6	79.3	78.2	82.1	81.2
4	84.6	80.5	79.8	78.6	82.3	80.9
5	84.5	80.1	79.0	78.8	81.8	81.3
6	84.8	80.8	79.1	78.0	82.2	81.0

3.4 XPS analysis

XPS measurements were performed to gain information about the membrane surface compositions, where solution-cast, hot-compression molded and thermally annealed membranes with 8% GO loading were utilized. Fit of the C1s spectra was conducted and the results are shown in Fig. 7. While C1s XPS spectrum for PVDF peaks at 290.9 and 286.4 eV, corresponding to the carbons of CF_2 and CH_2, respectively, that of GO shows four components arising from C–C (~284.4 eV), C–O (epoxy and hydroxyl, ~286.5 eV), C=O (carbonyl, ~288.0 eV) and COO (carboxyl, ~289.0 eV) (Fig. 7A), Notably, hot-pressed membrane exhibits an obvious decrease in oxygen components compared to the solution cast one (Fig. 7B and 7C), indicating the restore of conjugated structures of graphene. Through further annealing, the oxygen components are continuously decreased, which can be ascribed to the GO reduction. Since temperature has significant effect on the GO reduction,[40,41] the relatively low temperature of 200 °C adopted herein makes the GO reduction extent at a comparatively low level.

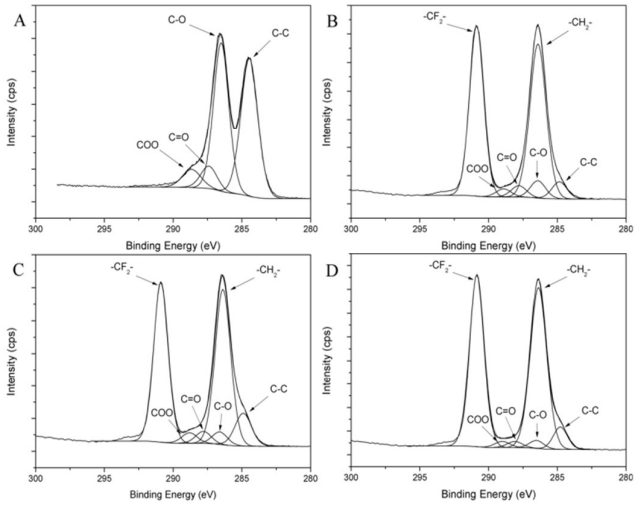

Fig. 7 High-resolution C1s XPS spectra of (A) GO (B) solution cast, (C) hot-compression molded and (D) annealed membranes with 8% GO.

3.5 Surface topography

Surface properties, particularly surface roughness are highly related to the contact angles. AFM topographic images reveal the surface variation of the composite membranes upon annealing. The mean roughness (R_a) of the composite membranes is slightly decreased from 6.93 to 5.87 nm after annealing (Fig. 8), which should be ascribed to the decrease in surface defect. It has been reported that the apparent contact angle increases with decreasing roughness to provide less surface wetting,[45] which might influence cellular adhesion behavior. Meanwhile, the hydrophilicity decrease (contact angle increase) after annealing can be attributed to the decrease of oxygen-containing hydrophilic groups and lowering of surface roughness, which will also affect the cell adhesion to the membrane.

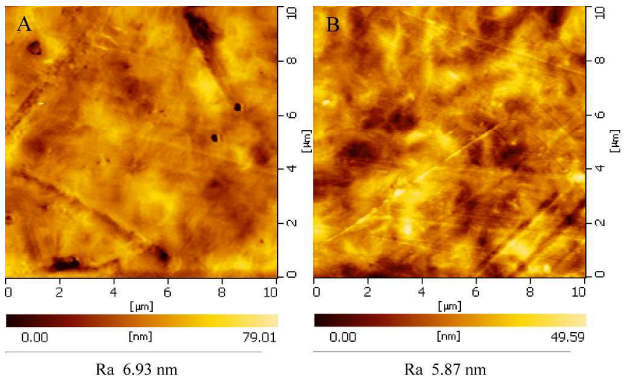

Fig. 8 AFM topographic images (height mode) for (A) G8, and (B) its further annealed membranes.

3.6 Cell adhesion and proliferation

PVDF membranes are widely used as biomaterials. Incorporation of RGO in PVDF greatly enhances its *β* phase fraction and

hydrophilicity, thus might be favorable for its biocompatibility and bioapplications. To check it, cell adhesion and proliferation on the membranes were carried out. Cell adherence to substrate is a vital process in tissue formation, cell differentiation and morphogenesis. HUVECs are widely used for biocompatibility tests owing to their cell anchorage-dependency. To ascertain the cell adhesion and proliferation behaviors on RGO/PVDF membranes, on which HUVECs were cultured and their dehydrogenase metabolic activities at various time intervals were monitored. For comparison, culture plates were also used as control. Optical density (OD) of the samples was measured to evaluate the cell viability. Each sample was measured three times (Table 2) and error bars are shown in Fig. 9（N=3, P<0.05）. Generally, higher OD means more living cells. Pristine PVDF membrane shows lowest ODs during the same culture period, indicating least cells and thus slowest HUVEC proliferation rate. Unlike it, RGO/PVDF membranes show approximate cell growth rate to that on the culture plate 3 d later. Additionally, the RGO content seems not significantly affect cell proliferation, as evidenced by the trivial difference of the OD values of G4 and G8 membranes. It is also noticeable that cell number on the annealed G8 membrane is the least after culture for 1 d; however, it is remarkably increased in the following days, and finally gets even more than those on the culture plate. Membrane hydrophilicity, surface roughness and composition may concurrently determine to the cell proliferation and proliferation behaviors.

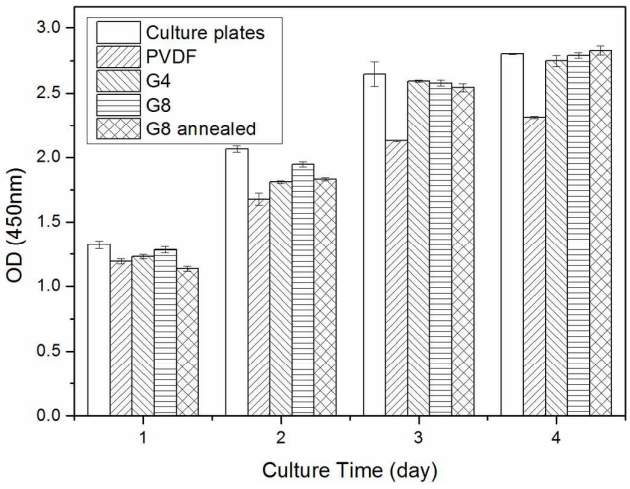

Fig. 9 Cell proliferation assay of HUVECs cultured on the composite membranes at different culture time. The optical density is monitored at 450 nm.

Table 2 Optical density of varying samples at different time

time (day)	culture plate	PVDF	G4	G8	G8 annealed
1	1.2946	1.1710	1.2184	1.2611	1.1154
	1.3169	1.2138	1.2233	1.2749	1.1312
	1.3565	1.1935	1.2468	1.3092	1.1556
2	2.0405	1.6883	1,8049	1.9622	1.8308
	2.0695	1.6256	1.8211	1.9232	1.8467
	2.0886	1.7185	1.8035	1.9554	1.8194
3	2.5470	2.1289	2.5896	2.5549	2.5100
	2.7323	2.1241	2.5859	2.5795	2.5715
	2.6582	2.1352	2.6000	2.6007	2.5475
4	2.8020	2.3180	2.7045	2.7707	2.8617
	2.7990	2.3096	2.7886	2.8074	2.7933
	2.7912	2.3028	2.7588	2.7965	2.8426

Further direct observation of the adhesion and proliferation of AO/EB stained HUVECs were carried out on a fluorescence microscope. Fig. 10 depicts the HUVECs cultivation results on membrane surfaces and culture plates for 2 h, 1 and 3 d, respectively. Apparently, HUVECs homogenously cover the culture plates after incubation for 3 d. Meanwhile, more cells are present on the composite membranes than on pure PVDF substrate, which confirms the proliferation assay result. HUVECs cultivated on culture plates and RGO/PVDF membranes show similar spindle-shape morphology, whereas those on pure PVDF substrate containing more polygonal cells. The elongated spindle-shape cell on graphene allows a higher proliferation.[31] It also noted that the cells are difficult to adhere to pure PVDF membranes, and prefer to attach the surface defects in the beginning of cultivation. The decreased surface roughness of the composite membranes might be the reason for lesser cells on themselves when compared with those on culture plates after being cultured for 1 d.

Fluorinated membranes are expected to resist cell attachment because of their hydrophobic nature.[46] However, addition of RGO increases the hydrophilicity of PVDF membranes, which is beneficial to the adhesion and proliferation of HUVECs. Moreover, RGO can promote the formation of *β* phase PVDF. Bouaziz et al. found that *β* phase PVDF substrate can stimulate endothelial cell secretion of prostacylin, which has anti-thrombotic functions.[47] Therefore, RGO/PVDF composite membranes are promising candidates as scaffold materials in tissue engineering for artificial blood vessel. More detailed studies, however, are needed to fully understand the interaction between cells and RGO/PVDF membranes.

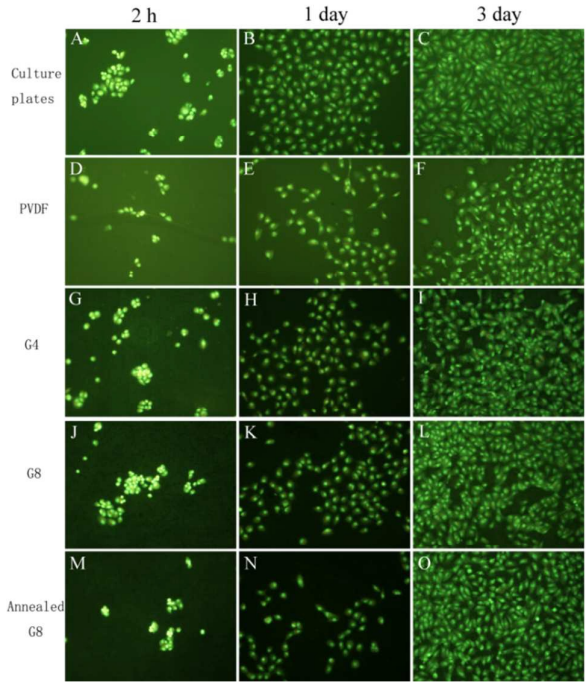

Fig. 10 Fluorescent photographs of HUVECs adhered to (A-C) culture plates, (D-F) pure PVDF, (G-I) G4, (J-L) G8, and (M-O) annealed G8 membranes for the culture of 2 h, 1 and 3 d, respectively (100×).

4 Conclusions

RGO/PVDF composite membranes with different RGO loadings

were prepared by a convenient in-situ thermal reduction method. Structural study reveals the good dispersion of RGO in the PVDF matrix. While pure PVDF only possess *α* phase crystals, incorporation of RGO results in the transformation from *α* to *β* phase, as indicated by the DSC and XRD results. Meanwhile, addition of RGO also effectively promotes the wettability of PVDF. Enhanced hydrophilicity and the formation of *β* phase PVDF are beneficial for achieving better biocompatibility: the adhesion and proliferation of HUVECs on the resulting composite membranes are promoted when compared to those on pure PVDF, at a comparable level to those on culture plates. Such results suggest the promising prospects of such composite membranes as biomaterials.

Acknowledgements

This work was financially supported by the National Natural Science Foundation of China (No. 21203118), the Shanghai Natural Science Foundation (No.15ZR1422100) and the Shanghai Leading Academic Discipline Project (No. B202).

Notes and references

1 A. K. Geim and K. S. Novoselov, *Nat. Mater.,* 2007, **6**, 183.
2 C. Soldano, A. Mahmood and E. Dujardin, *Carbon*, 2010, **48**, 2127.
3 Y. W. Zhu, S. Murali, W. W. Cai, X. S. Li, J. W. Suk, J. R. Potts and R. S. Ruoff, *Adv. Mater.*, 2010, **22**, 3906.
4 P. Chen, L. Guo and Y. Wang, *J. power sources*, 2013, **222**, 526.
5 X. M. Feng, Z. Z. Yan, N. N. Chen, Y. Zhang, Y. W. Ma, X. F. Liu,Q. L. Fan, L. H. Wang and W. Huang, *J. Mater. Chem. A*, 2013,**1**,12818.
6 Y. Liu, Q. H. Chang and L. Huang, *J. Mater. Chem. C*, 2013, **1**, 2970.
7 A. K. Yang, Y. Xue, Y. Zhang, X. F. Zhang, H. Zhao, X.J. Li, Y.J. H and Z. B. Yuan, *J. Mater. Chem. B*, 2013, **1**, 1804.
8 Y. Zhang, C. Y. Wu, X. J. Zhou, X. C. Wu, Y. Q. Yang, H. X. Wu, S. W. Guo and J. Y. Zhang, *Nanoscale*, 2013, **5**, 1816.
9 Y. Yu, Y. Liu, S. J. Zhen and C. Z. Huang, *Chem. Commun.*, 2013, **49**, 1942.
10 A. M. Pinto, I. C. Goncalves and F. D. Magalhaes, *Colloids Surf. B-Biointerfaces*, 2013, **111**, 188.
11 L. Zhang, W. W Liu, C. G. Yue, T. H. Zhang, P.Li, Z. W. Xing and Y. Chen, *Carbon*, 2013, **6**, 105.
12 H. X. Wang, D. M. Sun, N. N. Zhao, X. C.Yang, Y. Z. Shi, J.F. Li, Z. Q. Su and G. Wei, *J. Mater. Chem. B*, 2014, **2**, 1362.
13 W. H. Shang, X. Y. Zhang M. Zhang, Z. T. Fan, Y. T. Sun, M. Han and L. Z. Fan, *Nanoscale*, 2014, **6**, 5799.
14 W. Shao, H. Liu, X. F. Liu, S. X. Wang and R. Zhang, *RSC Adv.*, 2015, **5**, 4795.
15 J. H. Liu, T. C. Wang, H. F. Wang, Y. G. Gu, Y. Y. Xu, H. Tang, G. Jia and Y. F. Liu, *Toxicol. Res.*, 2015, **4**, 83.
16 H. Kim, A. A. Abdala and C. W. Macosko, *Macromolecules*, 2010, **43**, 6515.
17 S. Stankovich, D. A. Dikin, G. H. B. Dommett, K. M. Kohlhaas, E. J. Zimney, E. A. Stach, R. D. Piner, S. T. Nguyen and R. S. Ruoff, *Nature*, 2006, **442**, 282.
18 U. Klinge, B. Klosterhalfen, A. P. Öttinger, K. Junge and V. Schumpelick, *Biomaterials*, 2002, **23**, 3487.
19 D. M. Correia, R. Goncalves, C. Ribeiro, V. Sencadas, G. Botelho, J.L.G. Ribelles and S. Lanceros-Mendez, *RSC Adv.*, 2014, **4**, 33013.
20 M. S. Shoicbet and T. J. McCarthy, *Macromolecules*, 1991, **24**, 982.
21 P. Wang, K. L. Tan, E. T. Kang and K. G. Neoh, *J. Membrane Sci*., 2002, **195**, 103.
22 S. Kaur, Z. Ma, R. Gopal, G. Singh, S. Ramakrishna and T. Matsuura, *Langmuir*, 2007, **23**, 13085.
23 A. Rahinpour, S. Madaeni, S Zereshki and Y Mansourpanah, *Appl. Surf. Sic*., 2009, **255**, 7455.
24 T. Cai, W. J. Yang, K.G. Neoh and E. T. Kang, *Ind. Eng. Chem. Res*., 2012, **51**, 15962.
25 A. Cui, Z. Liu, C. Xiao and Y. Zhang, *J. Membrane Sci*., 2010, **360**, 259.
26 S. Huang, W. A. Yee, W. C. Tjiu,Y. Liu, M. Kotaki, Y. C. F. Boey, J.Ma, T. X. Liu and X. H. Lu, *Langmuir*, 2008, **24**, 13621.
27 Y. K. A. Low, N. Meenubharathi,N. D. Niphadkar, F. Y. C. Boey and K. W. Ng, *J. Biomater. Sci*., 2011, **22**, 1651.
28 J H. Yu, P. K. Jiang, C. Wu, L. C. Wang and X. F. Wu, *Polym. Comp*., 2011, **32**, 1483.
29 S. Ansari and E. P. Giannelis, *J. Polym. Sci. Polym. Phys*., 2009, **47**, 888.
30 M. Kalbacova, A. Broz, A. Kromka, O. Babchenko and M. Kalbac, *Carbon*, 2011, **49**, 2926.
31 M. Kalbacova, A. Broz, J. Kong and M. Kalbac, *Carbon*, 2010, **48**, 4323.
32 W. S. Hummers and R. E. Offeman, *J. Am. Chem. Soc*., 1958, **80**, 1339.
33 S. Stankovich, D. A. Dikin, R. D. Piner, K. A. Kohlhaas, A. Kleinhammes, Y. Jia, Y. Wu, T. Nguyen and R. S. Ruoff, *Carbon*, 2007, **45**, 1558.
34 S. Stankovich, D. A. Dikin, G. H. B. Dommett, K. M. Kohlhaas, E. J. Zimney, E. A. Stach, D. Piner, S. T. Nguyen and R. S. Ruoff, *Nature*, 2006, **442**, 82.
35 J. Zhang, H. Yang, G. Shen, P. Cheng, J. Zhang and S. Guo, *Chem. Commun*., 2010, **46**, 1112.
36 C. A. Amarnath, C. E. Hong, N.H. Kim, B. C. Ku, T. Kuila and J. H. Lee, *Carbon*, 2011, **49**, 3497.
37 Z. Fan, K. Wang, T. Wei, J. Yan, L. Song and B. Shao, *Carbon*, 2010, **48**, 1686.
38 Z. S. Wu, W. Ren, L. Gao, B. Liu, C. Jiang and H. M. Cheng,.*Carbon*, 2009, **47**, 493.
39 M. J. McAllister, J. L Li, D. H. Adamson, H. C. Schniepp, A. A. Abdala, J. Liu, M. Herrera-Alonso, D. L. Milius, R. Car, R. K. Prud'homme and I. A. Aksay, *Chem. Mater*., 2007, **19**, 4396.
40 H.C. Schniepp, J. L. Li, M. J. McAllister, H. Sai, M. Herrera-Alonso, D. H. Adamson, R. K. Prud'homme R. Car, D.A. Saville and I.A. Aksay, *J. Phys. Chem. B*, 2006, **110**, 8535.
41 S. F. Pei and H. M. Cheng, *Carbon,* 2012, **50**, 3210.
42 H. X. Tang, G. J. Ehlert, Y.R. Lin, H. A. Sodano, *Nano Lett.*, 2012,**12**,84.
43 Q. W. Li, L. B. Wang, Y. C. Zhu and Y. T. Qian, *Mater. Lett*., 2011, **65**, 2410.
44 A. C. Ferrari, J. C. Meyer, V. Scardaci, C. Casiraghi , M. Lazzeri, F. Mauri, S. Piscanec, D. Jiang, K. S. Novoselov, S. Roth and A. K. Geime, *Phys. Rev. Lett*., 2006, **97**, 187401.
45 T. S. Chow, *J. Phys. Condens. Matter*., 1998, **10**, L445.
46 G. Kim, H. Kim, I. J. Kim, J. R. Kim, J. I. Lee and M. Ree, *J. Biomater. Sci*., 2009, **20**, 1687.
47 A. Bouaziz, A. Richert and A. Caprani, *Biomaterials*, 1997, **18**, 107.

Fabrication and biocompatibility of reduced graphene oxide/poly(vinylidene fluoride) composite membranes

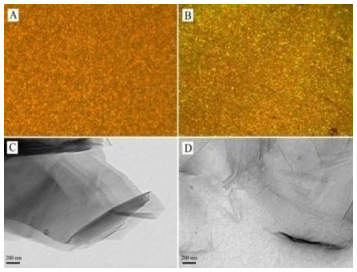

RGO/PVDF composite membranes with different RGO loadings were prepared by a convenient in-situ thermal reduction method and the structural study reveals the good dispersion of RGO in the PVDF matrix, moreover, RGO promotes the adhesion and proliferation of HUVECs on the resulting membranes, leading to the remarkably enhanced biocompatibility.